Bull. Chem. Soc. Ethiop. **2025**, 39(1), 29-47.
DOI: https://dx.doi.org/10.4314/bcse.v39i1.3

ISSN 1011-3924
Printed in Ethiopia
Online ISSN 1726-801X

FACILE SYNTHESIS OF ZnO/RGO/Fe_2O_3 USING MACROALGAE *Caulerpa taxifolia* AS GREEN REDUCTOR AND ITS APPLICATION AS MALACHITE GREEN REMOVAL

Said Ali Akbar[1*] and Muhammad Hasan[2]

[1]Department of Aquaculture, Faculty of Marine and Fisheries, Universitas Syiah Kuala, Banda Aceh, 23111, Indonesia
[2]Department of Chemistry Education, Faculty of Teacher Training and Education, Universitas Syiah Kuala, Banda Aceh, 23111, Indonesia

(Received January 30, 2024; Revised September 18, 2024; Accepted September 20, 2024)

ABSTRACT. This study presents the synthesis of a novel ZnO/rGO/Fe_2O_3 composite using *Caulerpa taxifolia* as a green reductant for the effective removal of Malachite Green from aqueous solutions. Characterization techniques, including FTIR, SEM, and XRD, confirmed the successful incorporation of ZnO and Fe_2O_3 onto the rGO matrix, enhancing its adsorption properties. The composite achieved an exceptional maximum adsorption capacity of 454.5 mg/g at pH 9, significantly outperforming rGO alone and other adsorbents. The adsorption kinetics followed a pseudo-second-order model, indicating chemisorption as the dominant mechanism, with a high correlation coefficient (R^2 = 0.999). The adsorption isotherms were best described by the Langmuir model, suggesting monolayer adsorption. Thermodynamic parameters revealed that the process was spontaneous and exothermic, with a Gibbs free energy (ΔGo) of -10.93 kJ/mol at 25 °C. The composite's high adsorption capacity, rapid kinetics, and favorable thermodynamics highlight its potential as an efficient and sustainable adsorbent for dye removal. This research offers a promising approach to water treatment, aligning with environmentally friendly practices and providing a viable solution for mitigating water pollution caused by organic dyes.

KEY WORDS: Reduced graphene oxide, Water treatment, *Caulerpa taxifolia*, Isothermal and kinetic studies, Malachite Green

INTRODUCTION

Water pollution is a pressing global issue, with organic dyes being among the most hazardous contaminants in aquatic environments [1]. Malachite Green (MG) is extensively used in various industries including textiles, leather, paper, and aquaculture [2]. Due to their synthetic origin and complex aromatic structures, they are resistant to biodegradation, posing significant environmental and health risks. Malachite Green, in particular, is known for its high toxicity, carcinogenicity, and potential to cause severe damage to aquatic ecosystems and human health. Consequently, the removal of such dyes from wastewater has become a critical area of environmental research [3].

Traditional wastewater treatment methods, such as coagulation, flocculation, and chemical oxidation, are often ineffective or too costly for the complete removal of these dyes [4, 5]. Therefore, adsorption has emerged as one of the most effective and economical methods for the removal of dyes from aqueous solutions [6]. This technique offers several advantages, including simplicity of operation, low cost, high efficiency, and the ability to handle large volumes of effluents [7, 8]. The effectiveness of adsorption largely depends on the properties of the adsorbent material, prompting extensive research into the development of novel adsorbents with high capacity and selectivity.

Graphene oxide (GO) and its reduced form, reduced graphene oxide (rGO), have attracted significant attention as promising adsorbent materials due to their large surface area, rich functional groups, and unique two-dimensional structure. The oxygen-containing functional

*Corresponding authors. E-mail: saidaliakbar@usk.ac.id

groups on GO, such as hydroxyl, epoxy, and carboxyl groups, provide active sites for the adsorption of dye molecules [9]. However, the performance of GO can be further enhanced by reducing it to rGO, which has fewer oxygen groups and a more restored sp^2 carbon network, improving its conductivity and mechanical strength. Despite these improvements, rGO alone may still have limitations in terms of adsorption capacity and selectivity [10].

To address these limitations, researchers have explored the modification of GO and rGO with various metal oxides to enhance their adsorption properties. Among these, zinc oxide (ZnO) and iron oxide (Fe_2O_3) have shown great potential due to their high surface area, magnetic properties, and ability to provide additional active sites for adsorption [11]. The incorporation of ZnO and Fe_2O_3 onto rGO not only improves the adsorption capacity but also facilitates the separation and recovery of the adsorbent after use [12, 13]. This composite approach combines the advantages of each component, resulting in a multifunctional material with superior performance.

The use of natural reducing agents in the synthesis of rGO-based composites has gained increasing interest due to their eco-friendliness, cost-effectiveness, and the potential to introduce additional functional groups onto the adsorbent surface. *Caulerpa taxifolia*, a marine macroalgae, has been identified as an effective green reductant for the synthesis of rGO [14]. Rich in bioactive compounds such as phenolics, flavonoids, and terpenoids, *Caulerpa taxifolia* not only aids in the reduction of GO to rGO but also introduces new functional groups that can enhance the adsorption of organic pollutants [15, 16]. The use of *Caulerpa taxifolia* as a green reductant offers a sustainable alternative to conventional chemical reducing agents, aligning with the principles of green chemistry [14, 17].

In this study, we synthesized a novel ZnO/rGO/Fe_2O_3 composite using *Caulerpa taxifolia* as a green reductant and evaluated its efficiency in the adsorption of Malachite Green from aqueous solutions. The composite was characterized using various techniques, including Fourier transform infrared (FTIR) spectroscopy, scanning electron microscopy (SEM), X-ray diffraction (XRD), and gas chromatography-mass spectrometry (GC-MS) analysis. These characterizations provided insights into the structural and functional properties of the composite, confirming the successful incorporation of ZnO and Fe_2O_3 onto the rGO matrix.

EXPERIMENTAL

Materials

The chemicals used for analysis were graphite powder (200 mesh size), $KMnO_4$, H_2SO_4 97-98%, $NaNO_3$, H_2O_2 30%, NaOH, deionized water, ethanol, DPPH (2,2-diphenyl-2-picrylhydrazil), Silicon Oil, filter paper Whatman grade 42, HCl 37%, ascorbic acid, $HClO_4$, HF, $NaBH_4$, KI and $FeCl_3$. The macroalgae used in this research are simplicia *Caulerpa taxifolia*.

Preparation of graphene oxide (GO)

Graphene oxide (GO) was synthesized using a modified Hummers method with graphite powder (200 mesh) as the starting material [18]. The process was as follows: 1 g of graphite, 0.5 g of sodium nitrate ($NaNO_3$), and 23 mL of concentrated sulfuric acid (H_2SO_4) were combined in a 500 mL flask. The mixture was stirred continuously while being maintained at 5 °C in an ice bath for 30 min. Next, 3 g of potassium permanganate ($KMnO_4$) was slowly added to prevent a vigorous localized reaction. After maintaining the reaction at 5 °C for two hours, the temperature was gradually raised to 35 °C with vigorous stirring for an additional 30 min. To the suspension, 100 mL of deionized water was added, causing the temperature to increase to 95 °C due to the hydration process. This temperature was held for 30 min with constant stirring. Subsequently, a mixture of 10 mL of 10% hydrogen peroxide (H_2O_2) and 90 mL of deionized water was added to complete the reaction. The resulting brownish-yellow product was isolated by vacuum filtration,

washed five times with deionized water and diluted HCl (5%, 200 mL) to remove Mn ions and any residual acid. The GO powders were then air-dried in an oven at 60 °C for 12 hours.

Preparation of plant extracts

Fresh and healthy leaves of *Caulerpa taxifolia* were collected from the Ulee Lheue Beach coastal area, Banda Aceh City, Aceh, Indonesia. The leaves were thoroughly washed under running water to remove any dirt or debris, followed by two additional rinses with distilled water. The cleaned leaves were then dried in a hot air oven at 85 °C for four hours [14]. Once dried, the leaves were finely ground into a powder. A 5 g portion of this powder was dissolved in 50 mL of distilled water and heated to 80 °C for one hour. After allowing the solution to cool, it was filtered using Whatman grade 42 filter paper to obtain the leaf extract.

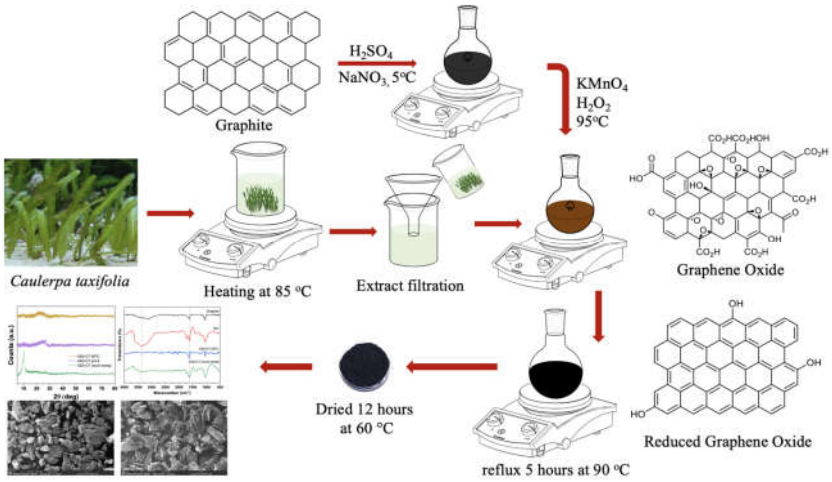

Figure 1. Systematic illustration of rGO synthesis.

Preparation of reduced graphene oxide (rGO)

In a 250 mL boiling flask, 100 mg of the synthesized GO powder was dispersed in 30 mL of demineralized water and subjected to ultrasonication for 30 min. To this mixture, 20 mL of *Caulerpa taxifolia* extract (0.1 g/mL) was added, and the solution was then heated under reflux at 90 °C for 5 hours [18]. During the formation of rGO, the mixture's color changed from dark brown to black. The resultant mixture was then centrifuged, and the precipitate was washed with hot demineralized water to remove any residual *Caulerpa taxifolia* extract. The final product was dried in a hot air oven at 60 °C for 12 hours to obtain the black powder of rGO (Figure 1).

Synthesis of ZnO/RGO/Fe_2O_3

The ZnO/RGO/Fe_2O_3 composite was synthesized by a hydrothermal method with modification [11, 12]. Initially, 100 mg of the previously prepared rGO was dispersed in 50 mL of demineralized water through ultrasonication for 30 min to ensure a uniform suspension. Subsequently, 0.5 g of zinc nitrate hexahydrate ($Zn(NO_3)_2 \cdot 6H_2O$) and 0.5 g of ferric nitrate nonahydrate ($Fe(NO_3)_3 \cdot 9H_2O$) were added to the rGO suspension with continuous stirring. The

mixture was then transferred to a Teflon-lined stainless-steel autoclave and heated at 180 °C for 12 hours to promote the hydrothermal reaction. After the reaction, the autoclave was allowed to cool to room temperature. The resulting ZnO/RGO/Fe_2O_3 composite was collected by centrifugation, washed several times with demineralized water and ethanol to remove any unreacted precursors, and then dried in a vacuum oven at 60 °C for 12 hours. The final product was a dark composite powder, which was further characterized for its structural and functional properties.

Characterizations

The *Caulerpa taxifolia* extract was analyzed using Fourier Transform Infrared (FTIR) spectroscopy (Bruker Alpha), a Thermo Scientific ISQ LT Single Quadrupole Mass Spectrometer, and a Thermo Scientific Trace 1310 Gas Chromatograph to identify the presence of functional molecules. Additionally, total phenol content and antioxidant activity were tested for further analysis. The morphology of both GO and rGO was examined using Thermo Scientific Axia ChemiSEM. The crystalline properties of GO and rGO were investigated through powder X-ray diffraction (XRD) using a Rigaku-Ultima IV (Japan) with nickel-filtered Cu–Kα radiation (λ = 0.154 nm). Functional group confirmation was performed using Fourier Transform Infrared (FTIR) spectroscopy with the Bruker Alpha instrument.

Adsorption procedure

A 50 mL sample solution of Malachite Green (MG) was prepared with concentrations ranging from 5 to 200 ppm. To each sample, 0.01 g of either rGO or ZnO/rGO/Fe_2O_3 was added. The mixture was stirred at 400 rpm for 20 min at ambient temperature (25 ± 2 °C). The residual MG concentration in the solution was then measured using UV-Vis spectroscopy (Shimadzu UV-3150) at a wavelength of 620 nm to generate a standard calibration curve.

$$\%\ Removal = \frac{C_0 - C_e}{C_0} \times 100\% \quad (1)$$

The formula to calculate the percentage removal of Malachite Green (or any adsorbate) shown in Equation (1), where C_0 is Initial concentration of Malachite Green (mg/L or ppm), C_e is equilibrium (or final) concentration of Malachite Green after adsorption (mg/L or ppm). This formula calculates the percentage of the initial concentration of Malachite Green that has been adsorbed and removed from the solution by the adsorbent.

Isothermal adsorption analysis

The Langmuir isotherm assumes monolayer adsorption on a homogeneous surface with a finite number of identical sites (Equation 2).

$$\frac{1}{q_e} = \frac{1}{Q_{max}\, K_L} . \frac{1}{C_e} + \frac{1}{Q_{max}} \quad (2)$$

where q_e is Amount of adsorbate adsorbed per unit mass of adsorbent (mg/g), Q_{max} is maximum adsorption capacity (mg/g), K_L is Langmuir constant related to the affinity of binding sites (L/mg), and C_e is equilibrium concentration of adsorbate in the solution (mg/L).

The Freundlich isotherm describes adsorption on a heterogeneous surface with different affinities for the adsorption sites (Equation 3).

$$\log q_e = \log K_f + \frac{1}{n}\log C_e \quad (3)$$

where q_e is Amount of adsorbate adsorbed per unit mass of adsorbent (mg/g), K_f is Freundlich constant indicating adsorption capacity [(mg/g)(L/mg)$^{(1/n)}$], n is heterogeneity factor (dimensionless), C_e is equilibrium concentration of adsorbate in the solution (mg/L).

The D-R isotherm describes adsorption on a heterogeneous surface and helps to distinguish between physical and chemical adsorption processes (Equation 4).

$$\ln q_e = \ln q_D - \beta\varepsilon^2 \quad (4)$$

where q_e is amount of adsorbate adsorbed per unit mass of adsorbent (mg/g), q_D is theoretical saturation capacity (mg/g), β is activity coefficient related to mean adsorption energy (mol²/J²), and ε is Polanyi potential, calculated as $\varepsilon = RTln\left(1+\frac{1}{C_e}\right)$ where R is universal gas constant (8.314 J/mol·K), T is temperature (K), and C_e is equilibrium concentration of adsorbate in the solution (mg/L).

Kinetics of adsorption

The pseudo-first-order model assumes that the rate of occupancy of adsorption sites is proportional to the number of unoccupied sites. It is commonly used for describing the kinetics of adsorption processes where physical adsorption is the dominant mechanism (Equation 5).

$$\log(q_e - q_t) = \log q_e - \frac{K_1}{2.303}t \quad (5)$$

where q_t is amount of adsorbate adsorbed at time t (mg/g), q_e is amount of adsorbate adsorbed at equilibrium (mg/g), K_1 is pseudo-first-order rate constant (min^{-1}), t is time (min).

The pseudo-second-order model assumes that the adsorption process may involve chemisorption, where the rate-limiting step involves valency forces through sharing or exchange of electrons between adsorbent and adsorbate (Equation 6).

$$\frac{t}{q_t} = \frac{1}{K_2 q_e^2} + \frac{t}{q_e} \quad (6)$$

where q_t is amount of adsorbate adsorbed at time t (mg/g), q_e is amount of adsorbate adsorbed at equilibrium (mg/g), K_2 is pseudo-second-order rate constant (g/mg·min), and t is time (min).

Adsorption thermodynamics

To determine the enthalpy (ΔH^o) and entropy (ΔS^o) changes, the Van't Hoff equation is used. It relates the equilibrium constant to temperature and provides a linear relationship when plotted (Equation 7).

$$\ln K_D = \frac{\Delta S^o}{R} - \frac{\Delta H^o}{RT} \quad (7)$$

where K_D is equilibrium constant (dimensionless), ΔH^o is standard enthalpy change (kJ/mol), ΔS^o is standard entropy change (kJ/mol·K), R is universal gas constant (8.314 J/mol·K), and T is temperature (K).

The relationship between the equilibrium constant and the standard Gibbs free energy change is given by Equation 8:

$$\Delta G^o = -RT \ln K_D \quad (8)$$

where ΔG^o is standard Gibbs free energy change (kJ/mol), R is universal gas constant (8.314 J/mol·K), T is temperature (K), and K_D is equilibrium constant (dimensionless).

RESULTS AND DISCUSSION

Total phenolic content and antioxidant activity

The analysis of *Caulerpa taxifolia* showed a total phenolic content of 4.48 ± 0.04 mg GAE/g, indicating the presence of phenolic compounds, which are known for their antioxidant properties. The antioxidant activity of the extract was evaluated using the IC_{50} value, which was found to be 12.31 mg/L. This suggests that the extract possesses a significant antioxidant potential, albeit slightly less effective than the standard, vitamin C, which has an IC_{50} value of 10.58 mg/L. The phenolic content in *Caulerpa taxifolia* likely contributes to its antioxidant activity, as phenolic compounds are effective scavengers of free radicals [14, 17]. The inhibition percentage of the *Caulerpa taxifolia* extract was assessed at various concentrations ranging from 2 to 10 mg/L. The results demonstrated a concentration-dependent increase in the percentage of inhibition. At the lowest concentration of 2 mg/L, the inhibition was 8.33%, and it increased progressively, reaching 42.59% at 10 mg/L. This trend indicates that higher concentrations of the extract result in greater inhibition, which can be correlated to its antioxidant capacity. The increasing inhibition percentages align with the extract's ability to neutralize free radicals more effectively as the concentration increases [14].

These findings suggest that *Caulerpa taxifolia* contains bioactive compounds with significant antioxidant properties, which can contribute to its potential application in various fields, including the synthesis of nanocomposites for environmental remediation. The presence of phenolic compounds and their associated antioxidant activity could play a crucial role in enhancing the performance of materials like ZnO/RGO/Fe_2O_3 in applications such as dye adsorption and pollutant removal.

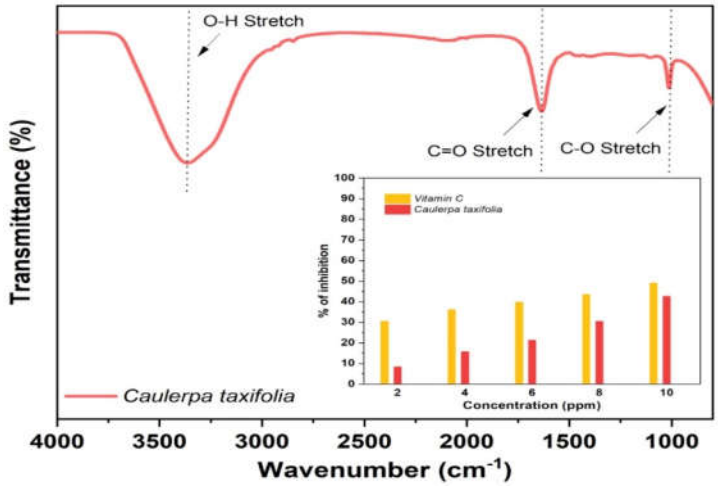

Figure 2. FTIR spectrum and inhibition properties of *Caulerpa taxifolia*.

FTIR analysis of Caulerpa taxifolia extract

The Fourier transform infrared (FTIR) spectroscopy analysis of *Caulerpa taxifolia* extract revealed several significant peaks, indicating the presence of various functional groups in the extract. These functional groups are crucial as they play a vital role in the reducing and stabilizing properties of the extract, which are important for applications in the synthesis of nanomaterials.

The peak observed at 1019 cm^{-1} corresponds to the C–O stretching vibration (Figure 2). This indicates the presence of alcohols, ethers, or esters in the extract, which are known to have good reducing properties. These compounds can act as reducing agents during the synthesis of nanoparticles, facilitating the reduction of metal ions into their respective nanostructures. A prominent peak at 1654 cm^{-1} is assigned to the C=O stretching vibration, which is associated with carbonyl groups [17]. The presence of this peak suggests that the carbonyl groups in the extract are conjugated with alkenes. Carbonyl compounds are known for their ability to interact with metal ions, which can aid in the stabilization of nanoparticles by forming complexes with the metal surfaces, thereby preventing aggregation. The broad peak around 3352 cm^{-1} indicates the presence of O–H stretching vibrations, characteristic of alcohols and phenols. The presence of hydroxyl groups enhances the reducing capacity of the extract, making it an effective agent for green synthesis processes [14]. Moreover, these hydroxyl groups can also facilitate the functionalization of nanoparticles, improving their dispersibility and interaction with target molecules, such as pollutants in water treatment applications.

Overall, the FTIR analysis confirms the presence of functional groups such as C–O, C=O, and O–H in the *Caulerpa taxifolia* extract. These groups contribute to its potential as a green reductant and stabilizing agent in the synthesis of nanomaterials, particularly for the creation of composites like ZnO/RGO/Fe_2O_3 for environmental remediation purposes.

GC-MS analysis of Caulerpa taxifolia extract

The GC-MS analysis of the *Caulerpa taxifolia* extract identified several bioactive compounds, each exhibiting significant biological activities such as antimicrobial and antibacterial properties. These compounds are likely to contribute to the overall bioactivity of the extract, which can be beneficial for various applications including the synthesis of nanocomposites and potential therapeutic uses.

One of the compounds identified was Tridecanoic acid, 12-methyl-, methyl ester, with a relative area of 0.697% and a retention time of 63.088 minutes. This compound is known for its antimicrobial properties [14], suggesting its potential use in preventing microbial growth in different environments. The presence of this compound in the extract indicates that *Caulerpa taxifolia* may have inherent antimicrobial capabilities, which can be advantageous when using this extract in materials intended for environmental or biomedical applications. Heptadecane was another major component, with a relative area of 16.594% and a retention time of 61.355 min. This compound is recognized for its antibacterial activity [17]. Its significant presence in the extract suggests that it might play a crucial role in the antibacterial efficacy of *Caulerpa taxifolia*, which could be useful in applications aimed at controlling bacterial contamination.

Cinnamic acid, 4-hydroxy-3-methoxy- (5-) was detected with a relative area of 0.528% and a retention time of 36.638 minutes. This compound also exhibits antimicrobial properties [17]. Cinnamic acid derivatives are well-known for their antimicrobial activity, which adds to the functional capabilities of the extract. Lastly, Z,E-2,13-Octadecadien-1-ol was identified with a relative area of 0.937% and a retention time of 3.437 min. This compound has antibacterial properties [14], indicating that it may contribute to the extract's ability to inhibit bacterial growth. In summary, the GC-MS analysis confirmed the presence of several bioactive compounds within the *Caulerpa taxifolia* extract, including those with known antimicrobial and antibacterial activities. These findings support the potential use of *Caulerpa taxifolia* extract as a bioactive

agent in the synthesis of nanocomposites, offering additional functional benefits such as microbial inhibition in environmental and medical applications.

The GO and rGO product analysis

XRD analysis

The X-ray Diffraction (XRD) analysis of the reduced graphene oxide (rGO) samples synthesized under different conditions revealed variations in their structural properties (Figure 3a). The rGO-CT sample synthesized at 90 °C exhibited a peak at 24.26°, corresponding to a d-spacing of 3.59 Å, indicative of the reduction of GO to rGO. This reduced interlayer spacing suggests the removal of some oxygen-containing groups and the restacking of graphene layers. However, the relatively broad peak (FWHM of 1.24) implies partial disorder or defects within the rGO layers, possibly due to incomplete reduction or residual functional groups.

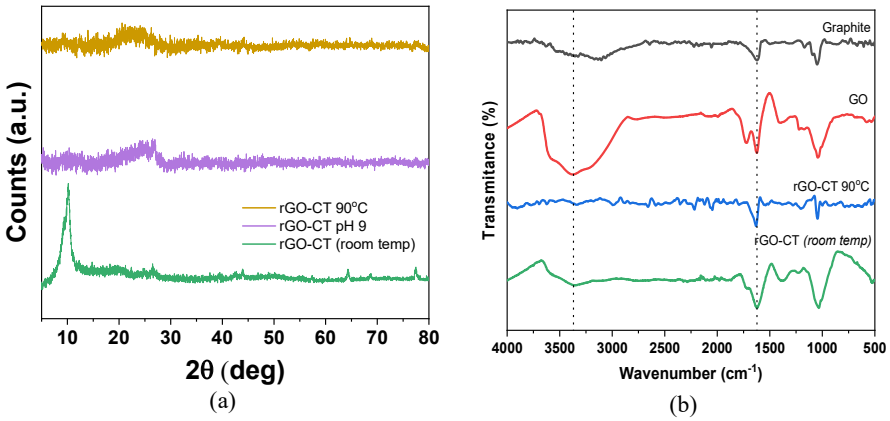

Figure 3. (a) XRD and (b) FTIR analysis of graphite, GO, and rGO.

The sample prepared at pH 9 showed a more distinct peak at 26.68°, with a smaller d-spacing of 3.33 Å, indicating a higher degree of reduction and improved graphitization compared to the 90°C sample. The lower d-spacing and sharper peak (FWHM of 1.10) suggest more effective removal of oxygen functionalities and a structure closer to that of pristine graphene, with higher crystallinity and fewer defects. In contrast, the sample synthesized at room temperature displayed a peak at 10.1°, characteristic of graphene oxide (GO) rather than rGO. This peak corresponds to a large d-spacing of 8.75 Å, indicating the presence of oxygen-containing groups and possibly intercalated water molecules, typical of GO structures [19]. Despite the relatively low FWHM value of 1.04, which usually suggests ordered layers, in this context, it indicates the presence of well-ordered GO rather than reduced graphene [20].

These results demonstrate that the synthesis conditions, particularly temperature and pH, significantly influence the reduction efficiency and structural properties of rGO. The rGO sample prepared at pH 9 exhibited the most successful reduction, resulting in a structure closely resembling graphene, while the room temperature synthesis was insufficient for complete reduction, maintaining the characteristics of GO.

FT-IR analysis

The Fourier transform infrared (FTIR) spectroscopy analysis reveals distinct differences in the functional groups present in graphite, graphene oxide (GO), and reduced graphene oxide (rGO)

samples synthesized at room temperature and at 90°C. These differences provide insight into the reduction process and the structural changes occurring in the material (Figure 3b).

In the GO spectrum, a broad peak was observed at around 3250 cm^{-1}, which corresponds to the O–H stretching vibrations. This peak is indicative of hydroxyl groups and possibly adsorbed water molecules, which are characteristic of GO due to the abundance of oxygen-containing functional groups [20]. The rGO-CT (room temperature) sample also displayed a broad peak at this wavenumber but with lower intensity, suggesting partial reduction of hydroxyl groups. This reduction implies that the oxygenated groups were not entirely removed during the reduction process at room temperature. Notably, this peak is absent in the spectra of graphite and rGO-CT synthesized at 90 °C, indicating the successful removal of hydroxyl groups in these samples, which reflects a more effective reduction process at higher temperatures. The peak at 1630 cm^{-1}, observed across all samples including graphite, GO, rGO-CT at 90 °C, and rGO-CT at room temperature, corresponds to the C=C stretching vibrations of aromatic rings. The presence of this peak in all spectra suggests that the sp^2 carbon network remains largely intact throughout the oxidation and reduction processes, maintaining the fundamental graphite-like structure [19].

A significant peak at 1717 cm^{-1} in the GO spectrum is associated with the C=O stretching vibrations of carbonyl groups, indicating a high level of oxidation in GO. The rGO-CT (room temperature) sample also shows a peak at this wavenumber, but with reduced intensity, suggesting that some carbonyl groups are still present but have been partially reduced. This indicates that the reduction at room temperature was not entirely effective in removing all carbonyl groups. In contrast, this peak is absent in the spectra of graphite and rGO-CT synthesized at 90°C, implying that the carbonyl groups were effectively reduced, resulting in a structure more similar to pristine graphite [18].

In summary, the FTIR analysis indicates that GO contains various oxygenated functional groups, including hydroxyl and carbonyl groups, which are partially reduced in rGO-CT at room temperature and more thoroughly reduced in rGO-CT at 90 °C. The absence of the broad O–H peak at 3250 cm^{-1} and the carbonyl peak at 1717 cm^{-1} in the rGO-CT 90 °C sample suggests a more complete reduction process, resulting in a material with fewer oxygenated groups and a structure closer to that of graphite. This emphasizes the importance of synthesis conditions in determining the efficiency of the reduction process and the resulting properties of rGO.

Microscopic studies

The Scanning Electron Microscopy (SEM) analysis provides a visual representation of the surface morphology and structural changes between graphene oxide (GO) and reduced graphene oxide (rGO). Figure 4 shows SEM images of GO and rGO at a magnification of 50x, highlighting the distinct morphological characteristics resulting from the reduction process.

In the SEM image of GO (Figure 4a), the structure appears as irregular, layered flakes with a relatively rough surface. These layers are stacked together but not tightly bound, which is typical of GO due to the presence of oxygen-containing functional groups that introduce defects and increase the interlayer spacing. The rough and wrinkled texture observed in the image is a result of the oxidation process, which adds functional groups like hydroxyl, epoxy, and carboxyl groups to the graphene sheets, disrupting the planar structure and creating a more disordered morphology [19].

In contrast, the SEM image of rGO (Figure 4b) displays a more compact and crumpled morphology with fewer visible gaps between the layers. This change in structure is indicative of the successful reduction of GO, where the removal of oxygenated groups leads to a decrease in interlayer spacing and restacking of the graphene sheets. The crumpled appearance suggests that the reduction process partially restores the π-π stacking interactions between the layers, leading to a more consolidated structure. However, the presence of some wrinkles and folds indicates that

the reduction is not entirely perfect, and some residual functional groups or defects may still be present [13].

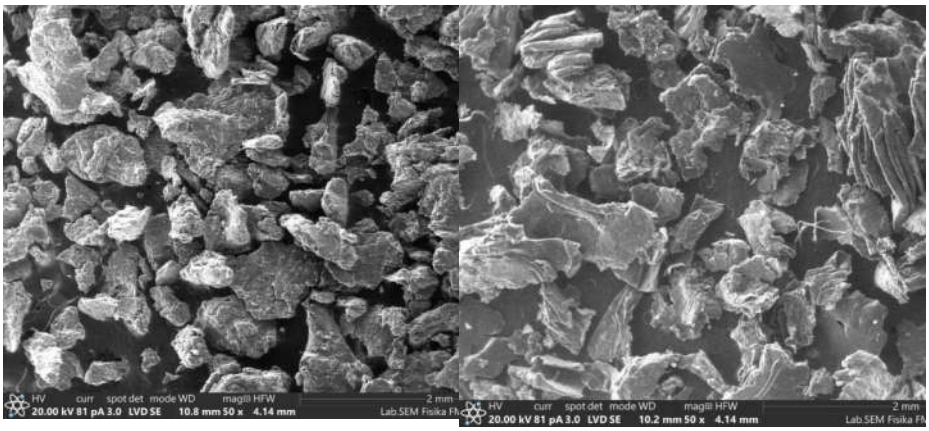

(a) (b)

Figure 4. SEM analysis with magnification 50x for (a) GO and (b) rGO.

Overall, the SEM analysis shows a clear transformation in the morphology from GO to rGO. The reduction process reduces the surface roughness and interlayer spacing, resulting in a more compact structure [21]. This morphological change is crucial as it directly impacts the properties of the material, such as its electrical conductivity, surface area, and potential applications in adsorption, catalysis, and other areas where reduced graphene oxide is utilized. The crumpled and layered structure of rGO also suggests enhanced potential for interactions with other materials or molecules, making it a versatile material for various applications.

Dye removal study

Effect of pH on removal efficiency of Malachite Green

The pH of the solution significantly impacts the adsorption process, particularly influencing the removal efficiency of Malachite Green (MG) when using rGO and ZnO/rGO/Fe_2O_3 as adsorbents. The data shows that as the pH increases from 3 to 11, there is a notable enhancement in the removal efficiency for both adsorbents. At lower pH values (pH 3-5), the removal efficiency of MG is relatively low for both adsorbents, with ZnO/rGO/Fe_2O_3 achieving efficiencies ranging from 26.65% to 62.76%, while rGO shows a lower efficiency ranging from 19% to 38.21%. The lower efficiency in acidic conditions can be attributed to the protonation of the adsorbent surface, leading to increased competition between H^+ ions and the cationic MG molecules for adsorption sites. Additionally, at lower pH, the surface of the adsorbents becomes more positively charged, which leads to electrostatic repulsion between the adsorbent and the positively charged MG molecules, reducing the adsorption capacity.

As the pH increases towards neutrality (pH 6-7), the removal efficiency shows a significant improvement. ZnO/rGO/Fe_2O_3 reaches up to 85.41% efficiency at pH 7, while rGO achieves 58.23%. This improvement can be explained by the deprotonation of the adsorbent surface, resulting in more negatively charged sites that enhance electrostatic attraction with the cationic MG molecules [18]. Additionally, the decrease in competition from H^+ ions allows for more efficient adsorption of MG onto the adsorbent surface. The removal efficiency reaches its peak in

the alkaline pH range (pH 8-11). ZnO/rGO/Fe_2O_3 demonstrates removal efficiencies above 92%, with a maximum of 96.08% at pH 11. Similarly, rGO shows a significant increase, with efficiencies rising from 65.32% at pH 8 to 73.58% at pH 11. The enhanced efficiency in alkaline conditions is due to the further increase in the negative charge density on the adsorbent surface, which promotes stronger electrostatic interactions with the positively charged MG molecules. Additionally, the alkaline environment may facilitate the interaction between MG and the functional groups on the adsorbents, leading to more effective adsorption [18, 21].

Overall, ZnO/rGO/Fe_2O_3 outperforms rGO alone in terms of removal efficiency across all pH levels, indicating that the incorporation of ZnO and Fe_2O_3 enhances the adsorption properties of the composite. This enhancement could be attributed to the increased availability of active sites and the synergistic effects between ZnO, Fe_2O_3, and rGO, which improve the interaction with MG molecules. Therefore, the optimal pH for the removal of Malachite Green using these adsorbents is in the alkaline range, specifically around pH 9 to 11. This pH range ensures maximum removal efficiency, making it ideal for applications in water treatment and dye removal processes.

Effect of temperature and contact time on removal efficiency of Malachite Green

The adsorption efficiency of Malachite Green onto rGO and ZnO/rGO/Fe_2O_3 was evaluated at different temperatures (25, 35, 45, and 55 °C) and various contact times. The results show a clear trend indicating the influence of temperature on the adsorption process for both adsorbents (Figure 5).

For rGO, the removal efficiency decreases with increasing temperature across all concentrations of Malachite Green. At a lower temperature of 25 °C, the removal efficiency is higher, reaching up to 73.58% at a concentration of 200 mg/L. However, as the temperature increases to 55 °C, the efficiency drops significantly, with a maximum removal efficiency of 50.22% at the same concentration. This trend suggests that the adsorption process for rGO is exothermic in nature, where higher temperatures reduce the adsorption capacity. The decrease in efficiency with rising temperature could be due to the increased kinetic energy of Malachite Green molecules, which disrupts the interaction between the dye and the adsorbent surface, leading to desorption. Additionally, higher temperatures may also result in a decreased affinity of the dye molecules for the active sites on rGO. In contrast, ZnO/rGO/Fe_2O_3 shows a relatively higher removal efficiency at lower temperatures but demonstrates a more gradual decline as the temperature increases. At 25 °C, the composite adsorbent achieves an exceptionally high removal efficiency of up to 96.34% at a concentration of 200 mg/L. Even at elevated temperatures of 55 °C, the efficiency remains substantial, with a maximum of 73.41% at the same concentration. The presence of ZnO and Fe_2O_3 in the composite appears to enhance the thermal stability and adsorption capacity, reducing the impact of temperature on the removal efficiency. This suggests that the adsorption process on ZnO/rGO/Fe_2O_3 might involve both physical and chemical interactions, where the chemical adsorption component is less affected by temperature changes [18].

The difference in temperature sensitivity between rGO and ZnO/rGO/Fe_2O_3 can be attributed to the nature of the interactions involved in the adsorption process. While rGO primarily relies on physical adsorption, including π-π interactions and van der Waals forces, ZnO/rGO/Fe_2O_3 benefits from additional chemical interactions, such as coordination with metal oxides. These interactions may provide more stable adsorption sites, leading to higher efficiency and reduced temperature dependence. In summary, lower temperatures (25-35 °C) are more favorable for achieving higher adsorption efficiency of Malachite Green for both rGO and ZnO/rGO/Fe_2O_3. ZnO/rGO/Fe_2O_3 demonstrates superior performance across the temperature range, indicating its potential as an effective adsorbent for dye removal even under varying thermal conditions. This temperature-dependent behavior is crucial for optimizing the adsorption process in practical applications,

where controlling the operating temperature can enhance the efficiency of dye removal in wastewater treatment.

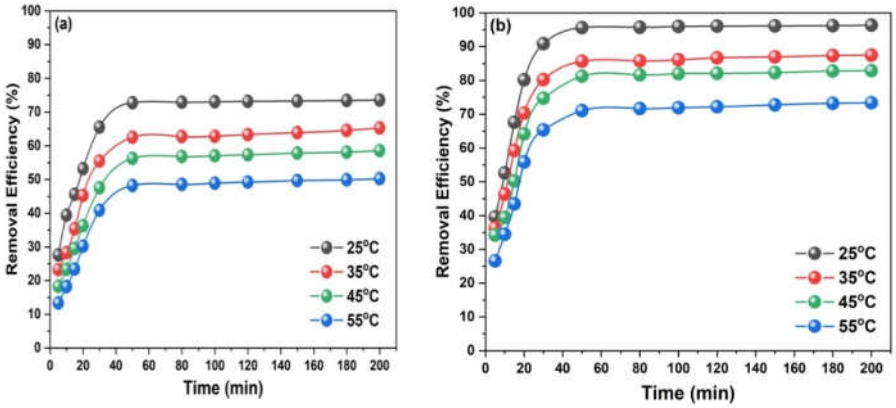

Figure 5. Effect of temperature and contact time on the removal efficiency of Malachite Green dye by (a) rGO and (b) ZnO/rGO/Fe_2O_3.

Isothermal adsorption analysis

The adsorption isotherms provide crucial insights into the interaction between Malachite Green and the adsorbents, rGO and ZnO/rGO/Fe_2O_3. By applying different isothermal models, we can better understand the adsorption mechanisms and the capacity of each adsorbent (Table 1).

The Langmuir isotherm model assumes monolayer adsorption onto a homogeneous surface with a finite number of identical sites. The maximum adsorption capacity (Q_{max}) for rGO was found to be 322.58 mg/g, whereas ZnO/rGO/Fe_2O_3 exhibited a significantly higher Q_{max} of 454.545 mg/g. This indicates that ZnO/rGO/Fe_2O_3 has a greater adsorption capacity, likely due to the synergistic effect of ZnO and Fe_2O_3 with rGO, providing more active sites and enhancing the interaction with Malachite Green molecules. The Langmuir constant (K_L) indicates the affinity between the adsorbent and the adsorbate. ZnO/rGO/Fe_2O_3 had a K_L value of 5.5 L/mg, much higher than that of rGO (0.492 L/mg), suggesting a stronger affinity and binding strength towards Malachite Green. This stronger affinity could be attributed to the combined effects of ZnO and Fe_2O_3, which potentially offer additional coordination and binding sites for the dye molecules. The separation factor (R_L) values for both adsorbents fall between 0 and 1 (rGO: 0.67–0.16, ZnO/rGO/Fe_2O_3: 0.153–0.017), indicating favorable adsorption. The R_L values of ZnO/rGO/Fe_2O_3 being closer to zero suggest a more favorable and efficient adsorption process compared to rGO.

Table 1. Isothermal adsorption parameters of malachite green on rGO and ZnO/rGO/Fe_2O_3.

Isothermal models	Quantities	rGO	ZnO/rGO/Fe_2O_3
Langmuir	Q_{max} (mg g^{-1})	322.58	454.545
	K_L (L/mg)	0.492	5.5
	R_L	0.67 – 0.16	0.153 – 0.017
Freundlich	n	1.63854	2.23214
	K_f(mg/g(L/mg)$^{1/n}$)	97.14454	399.0553
	R^2	0.971	0.9735
Dubinin Radushkevitch (D-R)	E (KJ/mol)	2.02196	5.8563
	q_D (mg/g)	194.9026	349.4289
	$B \times 10^{-6}$(mol^2/J^2)	0.1223	0.0181
	R^2	0.907	0.9309

The Freundlich isotherm model describes adsorption on heterogeneous surfaces and multilayer adsorption. The Freundlich constant (n) provides an indication of the adsorption intensity and favorability. The value of n for ZnO/rGO/Fe_2O_3 is 2.232, higher than that of rGO (1.639), implying that the adsorption process is more favorable on ZnO/rGO/Fe_2O_3. This suggests that the surface of ZnO/rGO/Fe_2O_3 is more heterogeneous, offering a range of adsorption sites with varying energies. The Freundlich constant (Kf) also reflects the adsorption capacity of the adsorbents. ZnO/rGO/Fe_2O_3 exhibits a much higher K_f value (399.1 mg/g(L/mg)$^{1/n}$) than rGO (97.14 mg/g(L/mg)$^{1/n}$), indicating its superior adsorption capability. The higher Kf value confirms that ZnO/rGO/Fe_2O_3 has a greater adsorption affinity and capacity for Malachite Green.

The Dubinin-Radushkevitch isotherm provides information on the adsorption energy and the nature of the adsorption process. The mean free energy (E) values indicate the type of adsorption mechanism. For rGO, E is 2.022 kJ/mol, while for ZnO/rGO/Fe_2O_3, E is 5.856 kJ/mol. Since these values are below 8 KJ/mol, it suggests that the adsorption of Malachite Green onto both adsorbents is primarily physisorption. However, the higher E value for ZnO/rGO/Fe_2O_3 implies a stronger interaction between the dye and the adsorbent compared to rGO. The adsorption capacity (qD) from the D-R model also highlights the superiority of ZnO/rGO/Fe_2O_3, with a q_D of 349.4289 mg/g, compared to 194.9 mg/g for rGO. This further confirms the enhanced adsorption capacity of ZnO/rGO/Fe_2O_3, likely due to its larger surface area and the additional adsorption sites provided by the incorporation of ZnO and Fe_2O_3.

Kinetic study of adsorption

The kinetics of adsorption were evaluated using pseudo-first-order and pseudo-second-order models to understand the adsorption mechanisms and the rate-controlling steps for rGO and ZnO/rGO/Fe_2O_3 (Table 2). The pseudo-first-order model assumes that the rate of occupation of adsorption sites is proportional to the number of unoccupied sites. For both rGO and ZnO/rGO/Fe_2O_3, the correlation coefficients (R^2) for the pseudo-first-order model ranged from 0.769 to 0.861, indicating a moderate fit to the experimental data. In rGO, the R^2 values for rGO increase slightly with temperature, from 0.795 at 25 °C to 0.861 at 55 °C. The rate constant K_1 varied between 0.020 and 0.026 min^{-1} across the temperature range. However, the theoretical adsorption capacity (q_e) calculated from this model is significantly lower than the experimental values, suggesting that the pseudo-first-order model does not adequately describe the adsorption process for rGO. Similarly, for ZnO/rGO/Fe_2O_3, the R^2 values range from 0.769 to 0.858, showing an increasing trend with temperature but still indicating a less-than-ideal fit. The rate constant K_1 values were slightly higher than those for rGO, ranging from 0.022 to 0.026 min^{-1}. The theoretical q_e values again did not match the experimental q_e values, indicating that the adsorption process may involve more complex interactions than those predicted by the pseudo-first-order model.

The pseudo-second-order model is based on the assumption that the rate-limiting step involves chemisorption, which includes electron sharing or exchange between adsorbent and adsorbate. This model provided a much better fit for both rGO and ZnO/rGO/Fe_2O_3, as indicated by the higher R^2 values. In rGO, The R^2 values for the pseudo-second-order model were exceptionally high (0.994 to 0.998) across all temperatures, indicating a strong correlation between the experimental data and the model. The rate constant K_2 decreased slightly with increasing temperature, ranging from 0.089 to 0.083 g/mg·min. The theoretical eqe values obtained from this model closely matched the experimental qeq_eqe values, suggesting that the adsorption process of Malachite Green onto rGO is predominantly governed by chemisorption mechanisms. For ZnO/rGO/Fe_2O_3, the pseudo-second-order model also showed excellent agreement with the [22–24] experimental data, with R^2 values ranging from 0.997 to 0.999. The K_2 values varied from 0.099 to 0.048 g/mg·min, showing a decreasing trend with increasing temperature. The theoretical q_e values were very close to the experimental values, indicating that chemisorption is the dominant mechanism for Malachite Green adsorption onto ZnO/rGO/Fe_2O_3. The higher q_e values compared

to rGO suggest that the incorporation of ZnO and Fe_2O_3 enhances the adsorption capacity, likely due to the introduction of additional active sites and the improvement of the adsorbent surface properties.

Table 2. Comparison of pseudo-first order and pseudo-second order kinetic parameters for rGO and ZnO/rGO/Fe_2O_3.

Adsorbent	Kinetic model	Parameter	25 °C	35 °C	45 °C	55 °C
rGO	Pseudo-first order	R^2	0.795	0.841	0.844	0.861
		K_1 (min^{-1})	0.020	0.026	0.025	0.025
		q_e theoretical (mg/mg)	0.412	0.431	0.359	0.351
		q_e experiment (mg/mg)	1.470	1.362	1.180	1.080
	Pseudo-second order	R^2	0.998	0.998	0.994	0.994
		K_2 (g/mg.min)	0.089	0.078	0.080	0.083
		q_e theoretical (mg/mg)	1.523	1.436	1.253	1.149
		q_e experiment (mg/mg)	1.470	1.362	1.180	1.080
ZnO/rGO/Fe_2O_3	Pseudo-first order	R^2	0.769	0.801	0.836	0.858
		K_1 (min^{-1})	0.022	0.025	0.026	0.026
		q_e theoretical (mg/mg)	0.389	0.403	0.484	0.644
		q_e experiment (mg/mg)	1.976	1.874	1.714	1.598
	Pseudo-second order	R^2	0.999	0.999	0.998	0.997
		K_2 (g/mg.min)	0.099	0.093	0.076	0.048
		q_e theoretical (mg/mg)	2.026	1.935	1.790	1.715
		q_e experiment (mg/mg)	1.976	1.874	1.714	1.598

The kinetic analysis indicates that the adsorption of Malachite Green onto both rGO and ZnO/rGO/Fe_2O_3 follows the pseudo-second-order kinetic model more closely than the pseudo-first-order model. This suggests that chemisorption is the primary mechanism, involving chemical interactions between the dye molecules and the adsorbent surface. The superior fit of the pseudo-second-order model is evidenced by the higher R^2 values and the close match between theoretical and experimental q_e values. The data also highlights that ZnO/rGO/Fe_2O_3 has a higher adsorption capacity and efficiency than rGO, indicating its potential as an effective adsorbent for dye removal in aqueous solutions.

Thermodynamic study of Malachite Green adsorption

The thermodynamic parameters, including the equilibrium constant (K_D), Gibbs free energy change ($\Delta G°$), enthalpy change ($\Delta H°$), and entropy change ($\Delta S°$), provide insights into the nature and spontaneity of the adsorption process (Table 3). The K_D values for rGO decrease with increasing temperature, from 2.773 at 25°C to 1.174 at 55°C. This decrease indicates that the adsorption capacity diminishes at higher temperatures, suggesting an exothermic nature of the adsorption process. For ZnO/rGO/Fe_2O_3, the K_D values are significantly higher than those for rGO, particularly at lower temperatures (e.g., 82.33 at 25°C), indicating a much higher adsorption capacity and affinity for Malachite Green. As with rGO, K_D decreases with increasing temperature, from 82.33 at 25°C to 3.98 at 55°C, again suggesting an exothermic process [25, 26].

The negative values of $\Delta G\circ$ across all temperatures indicate that the adsorption of Malachite Green onto rGO is spontaneous. However, as the temperature increases, $\Delta G\circ$ becomes less negative (from -2.53 kJ/mol at 25°C to -0.44 kJ/mol at 55°C), suggesting that the spontaneity of the process decreases with increasing temperature. This further supports the exothermic nature of the adsorption, where the process is more favorable at lower temperatures. The $\Delta G\circ$ values for ZnO/rGO/Fe_2O_3 are also negative, indicating a spontaneous adsorption process. These values are more negative than those for rGO, particularly at lower temperatures (-10.93 kJ/mol at 25°C),

suggesting a more favorable adsorption process. As temperature increases, ΔG° becomes less negative, decreasing from -10.93 kJ/mol to -3.76 kJ/mol, which indicates reduced spontaneity with rising temperature [27].

Table 3. Thermodynamic Parameters for the Adsorption of Malachite Green onto rGO and ZnO/rGO/Fe_2O_3.

Adsorbent	Temperature	K_D	ΔG°	ΔH°	ΔS°
rGO	25	2.773585	-2.52747	-24.1804	-0.07256542
	35	2.134796	-1.94197		
	45	1.439024	-0.96227		
	55	1.173913	-0.43725		
ZnO/rGO/Fe_2O_3	25	82.33333	-10.928	-81.9004	-0.2406321
	35	14.87302	-6.91277		
	45	5.993007	-4.73406		
	55	3.975124	-3.7634		

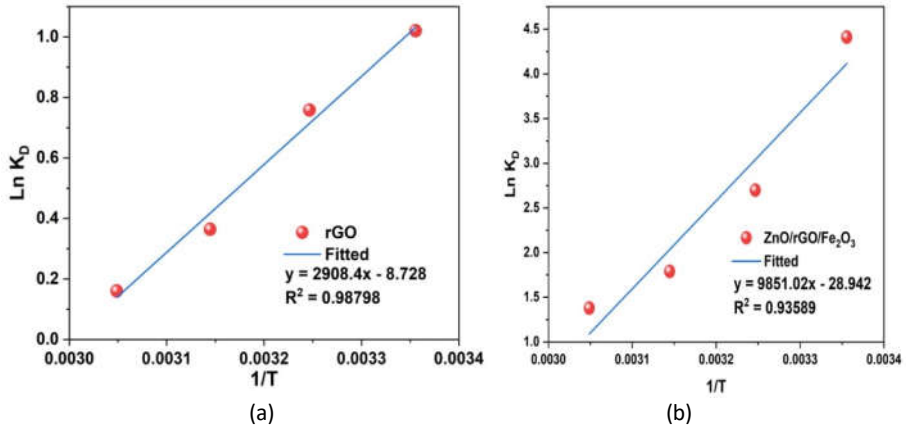

Figure 6. Ln K_D versus 1/T diagram for the sorption of malachite green dye at different temperatures with (a) GO and (b) ZnO/rGO/Fe_2O_3

The negative ΔH° value of -24.18 kJ/mol confirms that the adsorption is exothermic, meaning that heat is released during the adsorption process (Figure 6). This aligns with the observed trend that higher temperatures result in lower adsorption efficiency, as the process is less favorable when heat is applied. The negative ΔH° value of -81.90 kJ/mol is more negative than that for rGO, indicating a highly exothermic adsorption process. This substantial exothermicity implies that the adsorption onto ZnO/rGO/Fe_2O_3 involves stronger interactions, possibly due to the presence of ZnO and Fe_2O_3, which enhances the binding energy between the adsorbent and Malachite Green molecules [12].

The negative ΔS° value (-0.0726 kJ/mol·K) indicates a decrease in randomness at the solid-solution interface during the adsorption of Malachite Green onto rGO. This decrease in entropy suggests that the adsorbate molecules are more ordered on the surface of the adsorbent compared to their state in the bulk solution. The negative ΔS° value (-0.2406 kJ/mol·K) for ZnO/rGO/Fe_2O_3 is also more negative than that for rGO, suggesting a greater decrease in randomness at the solid-solution interface during adsorption. This further implies that the adsorption process is more

structured and ordered, likely due to the formation of more stable complexes between Malachite Green and the ZnO/rGO/Fe_2O_3 composite.

The thermodynamic analysis reveals that the adsorption of Malachite Green onto both rGO and ZnO/rGO/Fe_2O_3 is spontaneous and exothermic. ZnO/rGO/Fe_2O_3 exhibits a more favorable adsorption process, as indicated by higher K_D values, more negative ΔG°, and a greater negative ΔH^{o}, suggesting stronger interactions and a higher affinity for Malachite Green. The exothermic nature of the adsorption indicates that lower temperatures are more favorable for the process, with the degree of spontaneity decreasing as temperature increases. The negative entropy changes for both adsorbents imply an increase in orderliness at the interface, with ZnO/rGO/Fe_2O_3 showing a more significant decrease, likely due to more organized adsorption of Malachite Green molecules.

Comparison of adsorption capacities with other adsorbents

The comparison of ZnO/rGO/Fe_2O_3 synthesized with *Caulerpa taxifolia* with other adsorbents demonstrates its superior performance in terms of adsorption capacity for Malachite Green (Table 4).

Table 4. Comparison of adsorption capacities of different adsorbents for malachite green.

Adsorbent	Adsorption capacity (mg/g)	Condition			References
		pH	Concentration (mg/L)	Temp. (K)	
Lignin sulfonate-based mesoporous materials	121	7	100	308	[28]
Mg/Cr layered double hydroxide (LDH)	33.78	10	-	333	[29]
Chitosan bead	93.55	8	100	303	[30]
Bentonite	178.6	5	125	298	[31]
Zeolitic Imidazole Framework-8	224.1	7	200	303	[32]
Thiourea-modified poly (acrylonitrile-*co*-acrylic acid)	270	8	100	298	[33]
Acid-activated carbon—coconut shell	32.79	-	20	298	[34]
γ-Fe_2O_3/MWCNTs/Cellulose	47.61	-	-	298	[35]
ZnO/RGO/ Fe_2O_3—*Caulerpa taxifolia*	454.5	9	10	298	This work

With an adsorption capacity of 454.5 mg/g at pH 9 and a concentration of 10 mg/L, this adsorbent shows a significantly higher capacity than other materials reported in the literature. For example, thiourea-modified poly(acrylonitrile-co-acrylic acid) has a capacity of 270 mg/g at pH 8 and 298 K, while Zeolitic Imidazole Framework-8 (ZIF-8) exhibits 224.1 mg/g at pH 7 and 303 K. Traditional adsorbents such as activated carbon from lignite and bentonite have lower capacities, 200 mg/g and 178.6 mg/g, respectively. The enhanced performance of ZnO/rGO/Fe_2O_3 can be attributed to the synergistic effect of ZnO and Fe_2O_3 with reduced graphene oxide, which

offers a high surface area and abundant active sites for adsorption. This demonstrates the potential of ZnO/rGO/Fe_2O_3 as a highly efficient adsorbent for the removal of Malachite Green from aqueous solutions, outperforming other materials under similar conditions.

CONCLUSIONS

This study successfully demonstrated the synthesis of a novel ZnO/rGO/Fe_2O_3 composite using *Caulerpa taxifolia* as a green reductant, and its application in the removal of Malachite Green from aqueous solutions. The composite exhibited superior adsorption performance compared to rGO alone and other adsorbents reported in the literature, achieving a maximum adsorption capacity of 454.545 mg/g. This remarkable performance is attributed to the synergistic effects of ZnO and Fe_2O_3, which provide additional active sites, enhance the adsorption interactions, and introduce magnetic properties that facilitate easy separation and recovery of the adsorbent. Characterization studies using FTIR, SEM, XRD, and GC-MS confirmed the successful incorporation of ZnO and Fe_2O_3 onto the rGO matrix and the introduction of functional groups from the *Caulerpa taxifolia* extract. The adsorption kinetics followed a pseudo-second-order model, indicating that chemisorption is the dominant mechanism. The adsorption isotherms were best described by the Langmuir model, suggesting monolayer adsorption on a homogeneous surface. Thermodynamic analysis revealed that the adsorption process is spontaneous and exothermic, with a higher affinity and adsorption capacity at lower temperatures. The enhanced performance of ZnO/rGO/Fe_2O_3 underscores its potential as an effective adsorbent for the removal of toxic dyes like Malachite Green from wastewater. Its high adsorption capacity, rapid kinetics, and favorable thermodynamics make it a promising candidate for practical applications in water treatment. Additionally, the use of *Caulerpa taxifolia* as a green reductant aligns with sustainable and environmentally friendly practices, reducing the reliance on hazardous chemicals in the synthesis process. In summary, the ZnO/rGO/Fe_2O_3 composite synthesized in this study offers a multifunctional approach to addressing water pollution caused by organic dyes. Future research could explore the reusability and regeneration of this composite, as well as its application to a broader range of pollutants, to further establish its versatility and effectiveness in environmental remediation efforts. This work contributes to the development of sustainable, high-performance adsorbents for water purification, providing a pathway toward cleaner and safer water resources.

ACKNOWLEDGMENTS

We would like to thank the Indonesian Ministry of Research, Technology and Higher Education, which funded this research with contract number 660/UN11.2.1/PG.01.03/SPK/DRTPM/2024, tanggal 12 Juni 2024 through scheme *Penelitian Fundamental Reguler* (PFR). Apart from that, thank to the Marine Chemistry and Fisheries Biotechnology Laboratory, Faculty of Marine and Fisheries of Universitas Syiah Kuala, for encouraging this research's implementation. Lastly, thank you to the Research and Community Service (LPPM) of Universitas Syiah Kuala, Banda Aceh, Indonesia which has facilitated this program.

REFERENCES

1. Kubota, R.; Lyu, X.; Minami, T. Suppression of Malachite Green-induced toxicity to human liver cells utilizing host-guest chemistry of cucurbit[7]uril. *Anal. Sci.* **2021**, 37, 525-528.
2. Sharma, J.; Sharma, S.; Soni, V. Toxicity of Malachite Green on plants and its phytoremediation: A review. *Reg. Stud. Mar. Sci.* **2023**, 62, 102911.

3. Aziz, S.; Uzair, B.; Ali, M.I.; Anbreen, S.; Umber, F.; Khalid, M.; Aljabali, A.A.; Mishra, Y.; Mishra, V.; Serrano-Aroca, Á.; Naikoo, G.A.; El-Tanani, M.; Haque, S.; Almutary, A.G.; Tambuwala, M.M. Synthesis and characterization of nanobiochar from rice husk biochar for the removal of safranin and Malachite Green from water. *Environ. Res.* **2023**, 238, 116909.
4. Iqra; Khattak, R.; Begum, B.; Qazi, R.A.; Gul, H.; Khan, M.S.; Khan, S.; Bibi, N.; Han, C.; Rahman, N.U. Green synthesis of silver oxide microparticles using green tea leaves extract for an efficient removal of Malachite Green from water: Synergistic effect of persulfate. *Catalysts* **2023**, 13, 227.
5. Qaiyum, M.A.; Mohanta, J.; Kumari, R.; Samal, P.P.; Dey, B.; Dey, S. Alkali treated water chestnut (*Trapa natans* L.) shells as a promising phytosorbent for malachite green removal from water. *Int. J. Phytorem.* **2022**, 24, 822-830.
6. Chen, L.; Mi, B.; He, J.; Li, Y.; Zhou, Z.; Wu, F. Functionalized biochars with highly-efficient Malachite Green adsorption property produced from banana peels via microwave-assisted pyrolysis. *Bioresour. Technol.* **2023**, 376, 128840.
7. Gebreslassie, Y.T. Equilibrium, kinetics, and thermodynamic studies of Malachite Green adsorption onto fig (*Ficus cartia*) leaves. *J. Anal. Methods Chem.* **2020**, 2020, 7384675.
8. Ahmad, N.; Wijaya, A.; Arsyad, F.S.; Royani, I.; Lesbani, A. Layered double hydroxide-functionalized humic acid and magnetite by hydrothermal synthesis for optimized adsorption of malachite green. *Kuwait J. Sci.* **2024**, 51, 100206.
9. Xiao, D.; He, M.; Liu, Y.; Xiong, L.; Zhang, Q.; Wei, L.; Li, L.; Yu, X. Strong alginate/reduced graphene oxide composite hydrogels with enhanced dye adsorption performance. *Polym. Bull.* **2020**, 77, 6609-6623.
10. Han, M.; Xu, B.; Zhang, M.; Yao, J.; Li, Q.; Chen, W.; Zhou, W. Preparation of biologically reduced graphene oxide-based aerogel and its application in dye adsorption. *Sci. Total Environ.* **2021**, 783, 147028.
11. Sanei, A.; Dashtian, K.; Yousefi Seyf, J.; Seidi, F.; Kolvari, E. Biomass derived reduced-graphene-oxide supported α-Fe_2O_3/ZnO S-scheme heterostructure: Robust photocatalytic wastewater remediation. *J. Environ. Manage.* **2023**, 332, 117377.
12. Wang, X.; Li, Q.; Zhou, C.; Cao, Z.; Zhang, R. ZnO rod/reduced graphene oxide sensitized by α-Fe_2O_3 nanoparticles for effective visible-light photoreduction of CO_2. *J. Colloid Interface Sci.* **2019**, 554, 335-343.
13. Zhang, W.; Huang, H.; Bernstein, R. Zwitterionic hydrogel modified reduced graphene oxide/ZnO nanocomposite blended membrane with high antifouling and antibiofouling performances. *J. Colloid Interface Sci.* **2022**, 613, 426-434.
14. Akbar, S.A.; Hasan, M.; Afriani, S.; Nuzlia, C. Evaluation of phytochemical composition and metabolite profiling of macroalgae *Caulerpa taxifolia* and *C. peltata* from the Banda Aceh coast, Indonesia. *Biodiversitas* **2023**, 24, 5283-5292.
15. Akbar, S.A.; Mustari, A. Food packaging based on biodegradable polymers from seaweeds: a systematic review. *BIO Web Conf.* **2024**, 87, 01005.
16. Akbar, S.A.; Khairunnisa, K. Seaweed-based biosorbent for the removal of organic and inorganic contaminants from water: a systematic review. *BIO Web Conf.* **2024**, 87, 02011.
17. Akbar, S.A.; Hasan, M. Evaluation of bioactive composition and phytochemical profile of macroalgae *Gracilaria edulis* and *Acanthophora spicifera* from the Banda Aceh Coast, Indonesia. *Sci. Technol. Asia* **2024**, 29, 194-207.
18. Akbar, S.A.A.; Hasby, H. Synthesis of reduced graphene oxide using reducing lime juice (*Citrus aurantifolia*) and its application as Malachite Green adsorbent in aquatic environments. *J. Sci. Educ. Res.* **2023**, 9, 2229-2237.
19. Hessain, H.A.; Hassan, J.J. Green synthesis of reduced graphene oxide using ascorbic acid. *Iraqi J. Sci.* **2020**, 61, 1313-1319.
20. Muzyka, R.; Drewniak, S.; Pustelny, T.; Sajdak, M.; Drewniak, Ł. Characterization of graphite oxide and reduced graphene oxide obtained from different graphite precursors and

oxidized by different methods using Raman spectroscopy statistical analysis. *Materials* **2021**, 14, 769.
21. Manoratne, C.H.; Rosa, S.R.D.; Kottegoda, I.R.M. XRD-HTA, UV Visible, FTIR and SEM interpretation of reduced graphene oxide synthesized from high purity vein graphite. *Mater. Sci. Res. India* **2017**, 14, 19-30.
22. Qu, W.; Yuan, T.; Yin, G.; Xu, S.; Zhang, Q.; Su, H. Effect of properties of activated carbon on Malachite Green adsorption. *Fuel* **2019**, 249, 45-53.
23. Wang, M.; Jiao, Y.; Li, N.; Su, Y. Synthesis of a SiO_2-MgO composite material derived from yellow phosphorus slag with excellent Malachite Green adsorption activity. *J. Alloys Compd.* **2023**, 969, 172344.
24. Wu, J.; Yang, J.; Feng, P.; Wen, L.; Huang, G.; Xu, C.; Lin, B. Highly efficient and ultra-rapid adsorption of Malachite Green by recyclable crab shell biochar. *J. Ind. Eng. Chem.* **2022**, 113, 206-214.
25. Canayaz, M.; Aldemir, A.; Kul, A.R. Application of machine learning methods to removal percentage prediction for Malachite Green adsorption on kaolinite. *Desalination Water Treat.* **2022**, 247, 258-271.
26. Mohamed Omar, N.H.; Ahmad Zaini, M.A. Beta-cyclodextrin carbon microspheres by hydrothermal carbonization for Malachite Green adsorption. *Fuller. Nanotub. Carbon Nanostruct.* **2023**, 31, 182-189.
27. Hui, T.S.; Zaini, M.A.A. Textile sludge–sawdust chemically produced activated carbon: equilibrium and dynamics studies of Malachite Green adsorption. *Biomass Convers. Biorefin.* **2022**, 12, 2847-2859.
28. Tang, Y.; Zeng, Y.; Hu, T.; Zhou, Q.; Peng, Y. Preparation of lignin sulfonate-based mesoporous materials for adsorbing Malachite Green from aqueous solution. *J. Environ. Chem. Eng.* **2016**, 4, 2900-2910.
29. Palapa, N.R.; Badri, A.F.; Mardiyanto; Mohadi, R.; Taher, T.; Lesbani, A. Mg/Cr-$(COO)_2$-layered double hydroxide for Malachite Green removal. *Commun. Sci. Technol.* **2022**, 7, 91-97.
30. Bekçi, Z.; Özveri, C.; Seki, Y.; Yurdakoç, K. Sorption of malachite green on chitosan bead. *J. Hazard. Mater.* **2008**, 154, 254-261.
31. Bulut, E.; Özacar, M.; Şengil, I.A. Adsorption of Malachite Green onto bentonite: Equilibrium and kinetic studies and process design. *Micropor. Mesopor. Mater.* **2008**, 115, 234-246.
32. Khoshnamvand, N.; Jafari, A.; Kamarehie, B.; Mohammadi, A.; Faraji, M. Removal of malachite green dye from aqueous solutions using zeolitic imidazole framework-8. *Environ. Process.* **2019**, 6, 757-772.
33. Adeyi, A.A.; Jamil, S.N.A.M.; Abdullah, L.C.; Choong, T.S.Y. Adsorption of Malachite Green dye from liquid phase using hydrophilic thiourea-modified poly(acrylonitrile-co-acrylic acid): Kinetic and isotherm studies. *J. Chem.* **2019**, 2019, 4321475.
34. Piriya, R.S.; Jayabalakrishnan, R.M.; Maheswari, M.; Boomiraj, K.; Oumabady, S. Comparative adsorption study of malachite green dye on acid-activated carbon. *Int. J. Environ. Anal. Chem.* **2023**, 103, 16-30.
35. Khalatbary, M.; Sayadi, M.H.; Hajiani, M.; Nowrouzi, M. Adsorption studies on the removal of Malachite Green by γ-Fe2O3/MWCNTs/Cellulose as an eco-friendly nanoadsorbent. *Biomass Convers. Biorefin.* **2024**, 14, 2495-2513.